Available online at www.sciencedirect.com

SciVerse ScienceDirect

Ceramics International 38 (2012) 4337–4343

CERAMICS INTERNATIONAL

www.elsevier.com/locate/ceramint

# C/C–SiC–ZrC composites fabricated by reactive melt infiltration with $Si_{0.87}Zr_{0.13}$ alloy

Yiguang Wang *, Xiaojuan Zhu, Litong Zhang, Laifei Cheng

*Science and Technology on Thermostructure Composite Materials Laboratory, Northwestern Polytechnical University, Xi'an 710072, Shaanxi, PR China*

Received 19 December 2011; received in revised form 5 February 2012; accepted 7 February 2012
Available online 14 February 2012

**Abstract**

Carbon fiber reinforced carbon–silicon carbide–zirconium carbide (C/C–SiC–ZrC) composites were prepared by reactive melt infiltration (RMI) with $Si_{0.87}Zr_{0.13}$ alloy. Carbon fiber felt was firstly infiltrated by carbon using chemical vapour infiltration to obtain a porous carbon/carbon (C/C) skeleton. The molten $Si_{0.87}Zr_{0.13}$ alloy was then infiltrated into the porous C/C to obtain C/C–SiC–ZrC composites. The C–SiC–ZrC matrix showed a gradient structure with deposited carbon and SiC close to the fiber tows. It has been found that the C/C–SiC–ZrC showed a high strength, good oxidation resistance, and excellent ablation resistance. These properties are attributed to the gradient matrix structure.


*Keywords:* Ceramic–matrix composites (CMCs); Liquid metal infiltration (LMI); Formation mechanism

## 1. Introduction

Carbon fiber reinforced silicon carbide (C/SiC) has been considered as the most promising thermostructural material for applications in thermal protection system of the space vehicles as nose caps, leading edges, and ruddervator due to its excellent high-temperature strength, low density, good oxidation resistance and ablation resistance [1–5]. With the development of hypersonic space vehicles, the thermal protection system requires withstanding ultrahigh temperatures (>1800 °C) and high heat flux ablation [6]. C/SiC cannot meet the requirements because its rapid ablation at the scouring of the ultrahigh temperatures and high pressure flux will seriously limit the whole performance of the vehicles [7]. It is necessary to develop new composites with high ablation resistance in ultrahigh temperatures and oxidizing atmosphere.

One promising approach to improve the ablation resistance of C/SiC composites is to introduce refractory carbides/borides into the matrix or the coating. As result, the alternative ZrC–SiC multilayer coatings [8,9] and mixed $ZrB_2$–SiC coatings [10] have been fabricated. Several matrix-modified C/SiC systems including C/SiC–$ZrB_2$ [11,12], C/SiC–ZrC [13–15], C/SiC–TaC [16,17], C/SiC–$ZrB_2$–TaC [18] have been developed. Their ablation properties at ultrahigh temperatures were studied. The results indicated that the modified C/SiC composites showed better ablation resistance than C/SiC composites. However, the improvement in ablation is limited due to the low concentration of the refractory carbides/borides in the modified C/SiC composites. An alternative method to improve the ablation resistance of composites is to replace SiC matrix with refractory carbides/borides. The typical composite is C/ZrC that is fabricated by reactive melt infiltration (RMI) [19,20]. The ablation test in oxyacetylene flame showed that its linear ablation rate was about ten times lower than that of C/SiC [20]. Nevertheless, C/ZrC composites demonstrate a lower strength than C/SiC composites, which limits their application to the ultrahigh temperature thermostructure.

In this paper, C/C–SiC–ZrC composites were developed by RMI method with molten $Si_{0.87}Zr_{0.13}$ alloy. A unique structure was formed with fiber tows covered by deposited carbon and SiC, followed by gradient SiC–ZrC matrix. Such a structure results in good mechanical properties with the excellent oxidation resistance, while the ablation resistance has no obvious reduction compared to the C/ZrC composites.

## 2. Experimental procedure

Three-dimensional needled felt was fabricated by a needle-punching technique with alternatively stacked weftless piles

* Corresponding author. Tel.: +86 29 88494914; fax: +86 29 88494620.
*E-mail address:* wangyiguang@nwpu.edu.cn (Y. Wang).

0272-8842/$36.00 
doi:10.1016/j.ceramint.2012.02.016

(T-300™, Toray, Japan) and short-cut-fiber webs. The felt has a density of 0.52 g/cm$^3$ with a fiber volume of about 40%.

Carbon matrix was introduced into the felt by chemical vapour infiltration (CVI) at 960 °C using propane ($C_3H_6$) as precursor to form a porous C/C skeleton, followed by a graphitization process at 2400 °C for 1 h. The density of the porous preform was controlled to be approximately 1.4 g/cm$^3$ with an open porosity of 25%. The powder of $Si_{0.87}Zr_{0.13}$ alloy (Feret diameter 0.96 mm, Lihua Gaoke Chemical Company, Beijing, China) was molten in a pressure of 3 kPa at the temperature of 1800 °C. The composition of $Si_{0.87}Zr_{0.13}$ alloy is near to the eutectic point, at which the alloy has a low melting point. It will be helpful to reduce the infiltration temperature and thereby the damage of the fiber preform during the preparation. The molten $Si_{0.87}Zr_{0.13}$ alloy was infiltrated into the preform by capillary forces along the carbon fiber tow, where it reacted with the deposited carbon to form C–SiC–ZrC matrix. As comparison, C/C–ZrC composites were fabricated by RMI molten zirconium at 2000 °C using the same C/C porous preform [20].

The flexural strength of the composites was measured using a three-point bending test (SANS CMT 4304, Sans Testing Machine, Shen Zhen, China) with a span of 30 mm. At least three samples with a dimension of 40 mm × 5 mm × 3.5 mm were used for the test. The loading rate was 0.5 mm/min. The force–displacement curves were recorded by computer.

Thermogravimetric analysis (TGA) (Netzsch STA-409 C, Germany) was used to characterize the oxidation behavior of the C/C–SiC–ZrC composites. A small piece of composite was cut from the bulk for the oxidation process. During the temperature ramping process, ultra-high purity argon gas was used to protect the sample from oxidation. When the temperature reached the set value, several minutes were required to stabilize the temperature. After that, the dry air flowed into the chamber with a rate of 50 ml/min. The oxidation time was 60 min. The weight change was recorded by the computer as function of oxidation time. As comparison, the oxidation behavior of the C/C–ZrC composites that fabricated by RMI process was also tested in the same condition.

The ablation tests were carried out in a vertically jetted flowing oxyacetylene torch environment. The exposure time under the torch flame was 20 s. At least three samples with a dimension of Φ 30 mm × 5 mm were used in the test. Further detail about the test process was described elsewhere [10]. The temperature distribution on the sample surface was calculated using the FLUENT software based on the method of Gibbs free energy minimization. It was assumed that there was no friction between the flowing gas and equipment tube. The results showed that the heat flux was about 4200 kW/m$^2$ (±10% error) and the temperature in the center of the sample was about 3000 °C, which was in accordance with the measured temperature by the multiwavelength pyrometer [10,11].

The phases of the composites were analyzed by X-ray diffractometer (XRD, Rigaku D/max-2400, Tokyo, Japan) with Cu $K_\alpha$ radiation. Data were digitally recorded in a continuous scan mode in the angle ($2\theta$) range of 15–80° with a scanning rate of 0.12°/s. The microstructure of the specimens was observed by SEM. The elemental analysis was conducted by energy dispersive spectroscopy (EDS). The density of the samples was measured by the Archimedes method with distilled water.

## 3. Results and discussion

### 3.1. Microstructure of porous C/C and C/C–SiC–ZrC composites

Fig. 1 exhibits the microstructure of porous C/C. As can be seen, the carbon fibers are covered with a thick layer of pyrolytic carbon. In the carbon matrix, there are different sizes of apertures, which provide the infiltration channels for the molten $Si_{0.87}Zr_{0.13}$ alloy in the RMI process. The distribution of these apertures is shown in Fig. 2. The capillary diameters of these apertures are mainly in the range of 20–80 μm.

The XRD pattern of C/C–SiC–ZrC is shown in Fig. 3. The phases in the composites are mainly SiC, ZrC and C. A small amount of $ZrSi_2$, the residual of $Si_{0.87}Zr_{0.13}$ alloy, is also detected by XRD. The results indicate that most of the infiltrated $Si_{0.87}Zr_{0.13}$ alloy has reacted with carbon to form SiC–ZrC matrix.

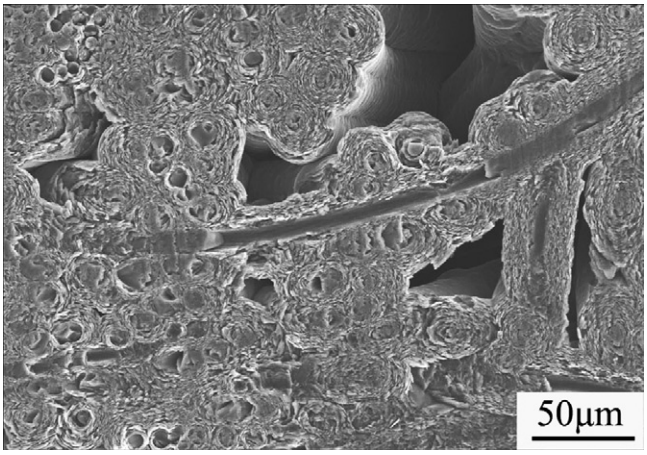


Fig. 1. Cross-section of the porous C/C skeleton.

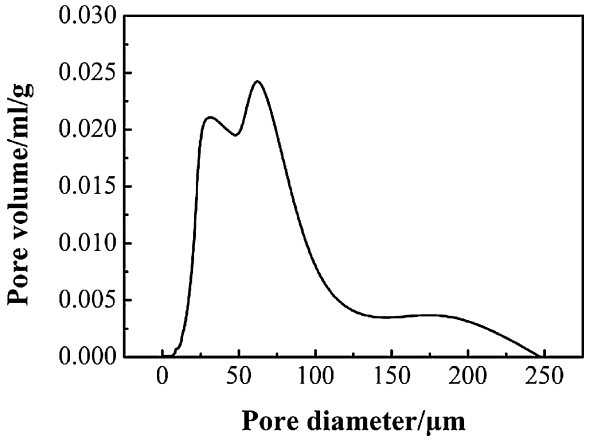


Fig. 2. Pore size distribution in the porous C/C skeleton.

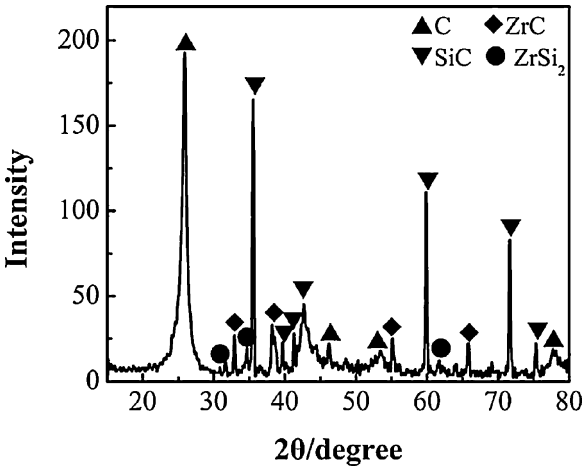


Fig. 3. XRD pattern of C/C–SiC–ZrC composites fabricated at 1800 °C for 30 min.

Fig. 4 shows a typical cross-section of C/C–SiC–ZrC composite. It is seen that the SiC–ZrC matrix (with a small amount of residual $ZrSi_2$) is formed deeply along the direction of 3D acupunctures. As seen from Fig. 4, the generated matrix is dense except a few of microscopic voids in it, and seals most of the pores inside the composites. The distribution of SiC–ZrC is not even, which is caused by the pores' distribution in C/C porous preform.

The detail microstructure of C/C–SiC–ZrC composites is shown in Fig. 5a. As can be seen, the deposited carbon covers the fiber tows, between which there is the formed SiC–ZrC matrix. EDS analysis was carried out from the spot near to the fiber bundle to the center of SiC–ZrC matrix (Fig. 5b–e). At the A-point near to the fiber bundle, there is only SiC formed as indicated in Fig. 5b. Far from A-point, ZrC begins to show in the matrix, the closer to the center of the matrix, the higher ZrC (Fig. 5c and d). At the center between two carbon bundles, it seems that the composition of the matrix is close to $ZrSi_2$ with only a little of carbon diffusion in (Fig. 5e). Accordingly, the architecture of the resultant C/C–SiC–ZrC can be described as a bundle of fiber covered by deposited carbon, followed by SiC, gradient SiC–ZrC matrix, and unreacted $ZrSi_2$ alloy.

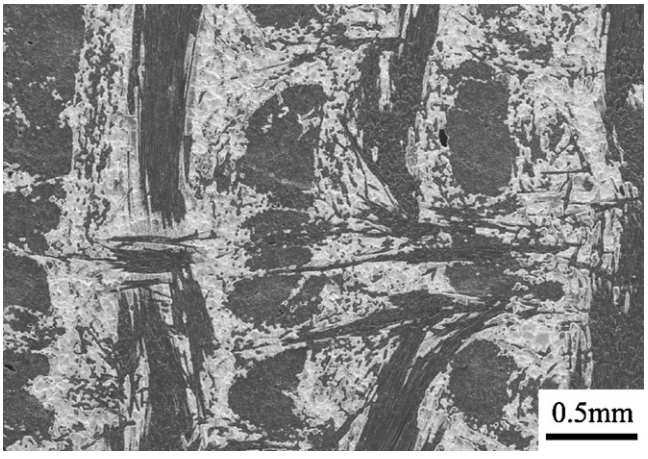


Fig. 4. Cross-section of C/C–SiC–ZrC composites fabricated at 1800 °C for 30 min.

### 3.2. The mechanism for the formation of C/C–SiC–ZrC composites

The reaction between $Si_{0.87}Zr_{0.13}$ alloy and deposited carbon can be discussed based on the Zr–Si–C ternary phase diagram. However, there is no Zr–Si–C phase diagram available at 1800 °C. We can refer to the Zr–Si–C phase diagram at 1700 °C instead (Fig. 6 [21]), in which the upper area of Si–$ZrSi_2$–SiC should be close to that at 1800 °C.

The circle point marked in the upper area in Fig. 6 is the $Si_{0.87}Zr_{0.13}$ alloy. According to the phase diagram, the $Si_{0.87}Zr_{0.13}$ melt will react with carbon to form SiC and $ZrSi_2$. Since $ZrSi_2$ is liquid at the temperature of 1800 °C [22], it will partially dissolve in the Si–Zr alloy to increase its concentration, and partially react with carbon to form the mixture of SiC–ZrC. Due to the low concentration of zirconium in $Si_{0.87}Zr_{0.13}$, the formed $ZrSi_2$ is less than SiC at the beginning, the ZrC originated from the reaction of $ZrSi_2$ with carbon should be much less than SiC. It is thus considered that a SiC layer is formed around the carbon at the beginning. As the SiC layer is built up, the carbon will diffuse through it to react with the Zr–Si melt. As the reaction is going further, the concentration of zirconium in the melt increases and more $ZrSi_2$ forms, the product of ZrC will increase in the SiC–ZrC matrix. This process leads to the gradient SiC–ZrC matrix in the final composites with a little of residual $ZrSi_2$, which coincides to the experimental observation.

In order to further verify this mechanism of formation gradient SiC–ZrC matrix, Si–Zr alloys with various compositions will be tried in the RMI process. Another composition of alloy between Si and $ZrSi_2$, $Si_{0.80}Zr_{0.20}$, was used in RMI process at 1800 °C. The similar gradient SiC–ZrC matrix was obtained. The Si–Zr alloys with higher zirconium concentration have to be tested in the future due to the limitation in treatment temperature of our present devices.

### 3.3. Mechanical properties of C/C–SiC–ZrC composites

The flexural load-displacement curve of C/C–SiC–ZrC composites is shown in Fig. 7. The C/C–SiC–ZrC composites shows pseudoplastic behavior, which attributes to the crack deflection (Fig. 8a), interfacial debonding and fiber pull-out (Fig. 8b). Fig. 8 also indicates that the fibers are well protected during RMI process.

The calculated bending strengths of these composites are listed in Table 1. C/C composites are the porous preforms used for fabricating C/C–ZrC and C/C–SiC–ZrC composites. Their density and strength are low. The obtained C/C–ZrC by RMI has high density. However, its strength is pretty low though the value is about twice of that of the C/C preform. According to the previous analysis [20], the C/C–ZrC is pretty dense and no obvious cracks. The low strength should mainly originate from the matrix itself rather than the defects in the composites. During the bending process, the generated cracks easily propagate

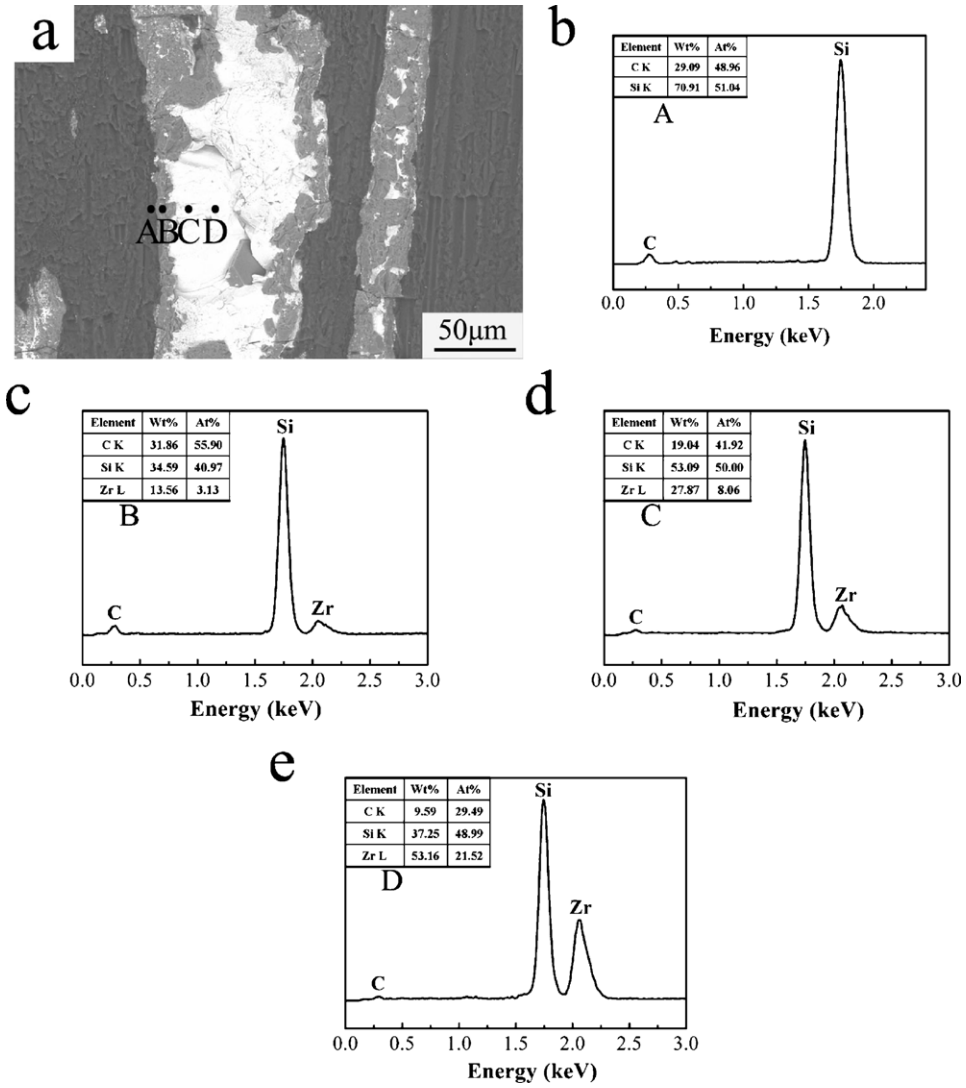


Fig. 5. Morphologies of the surface C/C–SiC–ZrC composites (a), and the EDS analysis of different spots (b)–(e).

through ZrC matrix to reach the carbon fibers, leading to the fracture at low strength. As to the C/C–SiC–ZrC composites, it has a structure of carbon fibers covered by the deposited carbon and SiC, followed by a gradient SiC–ZrC matrix.

The matrix in C/C–SiC–ZrC should have an increased gradient modulus from the center of matrix to the fiber tows due to the difference in Young's modulus of SiC (475 GPa) and ZrC (350–400 GPa) [24,25]. Because the Young's modulus of the

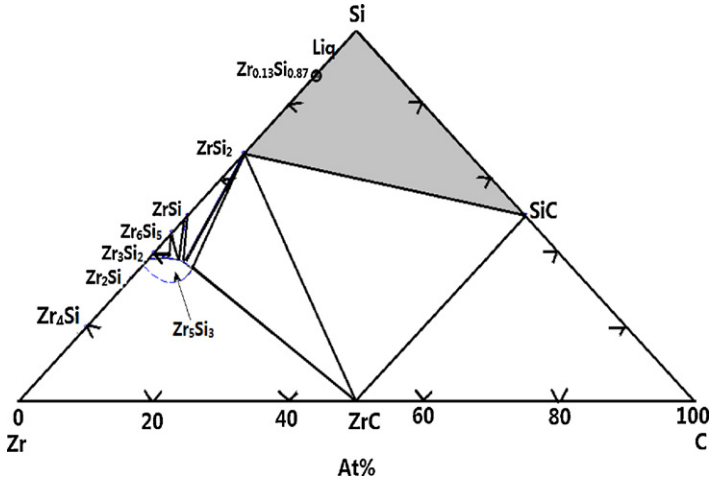


Fig. 6. Si–Zr–C ternary phase diagram [21].

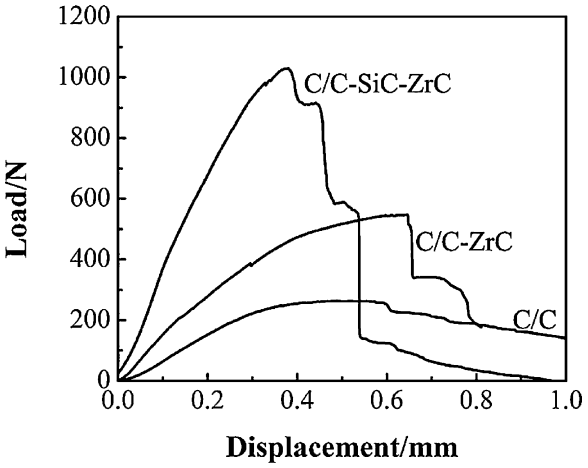


Fig. 7. Typical load-displacement curves of C/C composites, C/C–ZrC and C/C–SiC–ZrC composites.

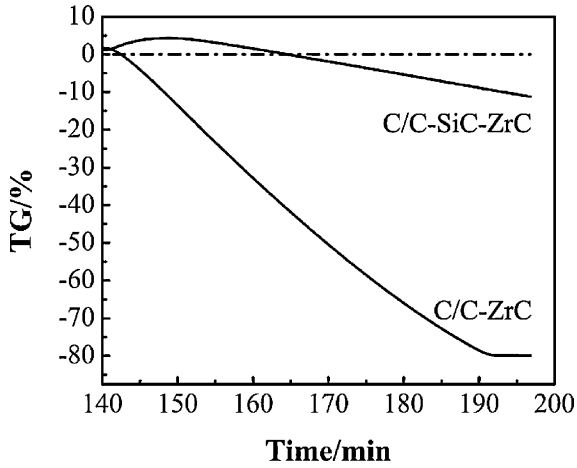


Fig. 9. The weight change of C/C–SiC–ZrC and C/C–ZrC as a function of time in the air at 1400 °C.

matrix at the center is smaller than that of the one close to the fiber tows, the stress of the crack tip will lower in virtue of the dispersion of the principal stress, making the stress of the crack tip too small to spread into the interior of the matrix [26]. Therefore, when the force applied on the SiC–ZrC matrix, the crack propagation will be suppressed due to the diffusion of the principal tensile stresses into the interior of the composite. The strength of C/C–SiC–ZrC is thus high. The in situ formed gradient matrix will enhance the damage tolerance of the composites.

### 3.4. Oxidation behavior of C/C–SiC–ZrC composites

The oxidation behaviors of the C/C–SiC–ZrC and C/C–ZrC were tested in air at 1400 °C. The weight change of these composites as a function of oxidation time is shown in Fig. 9. It is seen that the C/C–ZrC loses weight linearly up to 79% after oxidation for 1 h, while the C/C–SiC–ZrC gains weight at the beginning followed by weight loss up to 11% after 1 h. The C/C–SiC–ZrC shows a much better oxidation resistance than that of C/C–ZrC. In the oxidant environments, ZrC is oxidized to $ZrO_2$ that is a good oxygen-ion conductor at high temperatures. The oxygen can easily diffuse through $ZrO_2$ to consume carbon in the composites, causing the weight loss. As to the C/C–SiC–ZrC, the oxidation products include $SiO_2$ besides $ZrO_2$. $SiO_2$ is known as a good oxygen barrier, able to retard the diffusion of oxygen. At the beginning, the oxidation happens only at the matrix of SiC–ZrC, resulting in the weight gain. With the prolongation of the oxidation time, the carbon fibers will be oxidized, leading to the weight loss. However, due to the existence of protective silica layer, the oxidation rate is greatly reduced compared to C/C–ZrC composites.

### 3.5. Ablation behavior of C/C–SiC–ZrC composites

The macrographic pictures of C/C–SiC–ZrC before and after ablation test are shown in Fig. 10. A white layer can be

Table 1
The densities and calculated flexural strength of C/C, C/C–ZrC, C/C–SiC–ZrC and C/C–SiC composites.

| Composites | C/C | C/C–ZrC | C/C–SiC–ZrC | C/C–SiC [23] |
|---|---|---|---|---|
| Density (g/cm$^3$) | 1.39 ± 0.02 | 2.57 ± 0.03 | 2.35 ± 0.05 | 2.37 ± 0.02 |
| Flexural strength (MPa) | 63 ± 3 | 112 ± 5 | 205 ± 8 | 223 ± 6 |

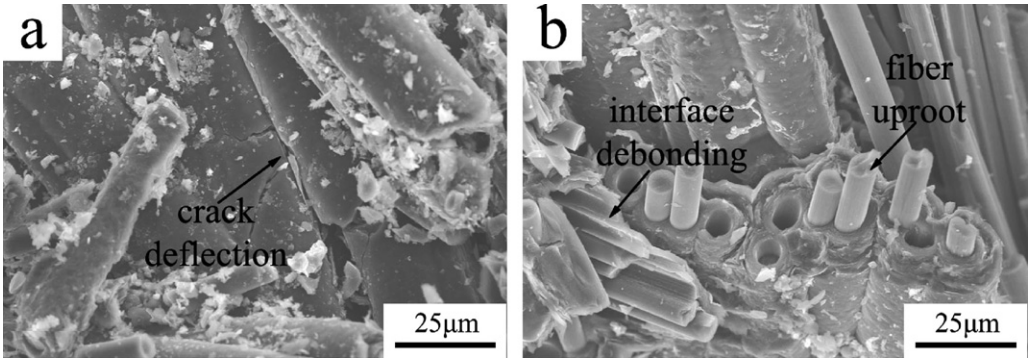


Fig. 8. The fracture surfaces of C/C–SiC–ZrC composites (a) crack deflection and (b) interface debonding and fiber uproot.

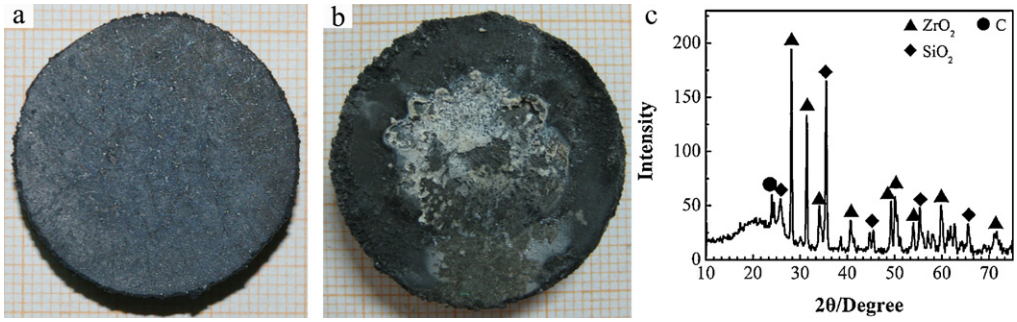


Fig. 10. Macrographic pictures of C/C–SiC–ZrC composites before (a) and after ablation (b), and XRD pattern of the ablated surface (c).

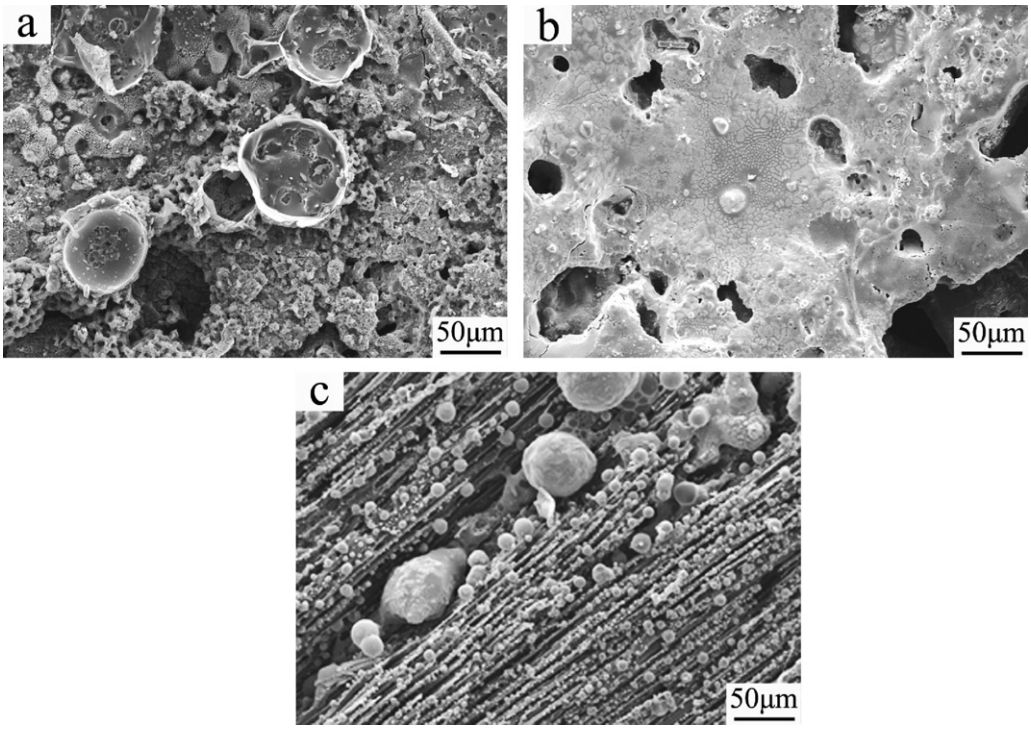


Fig. 11. Morphologies of the ablated surface in oxyacetylene flame. (a) The low-temperature region, (b) the region near to the ablation center, and (c) the center region.

found on the ablated surface of C/C–SiC–ZrC composites. XRD pattern of the surface on the ablated samples (Fig. 10c) indicates that the white layer consists of a mixture of $ZrO_2$ and $SiO_2$. The dimensional change of the samples before and after ablation test was measured to obtain the linear ablation rate. The value for C/C–SiC–ZrC is −0.004 mm/s. Compared to the values of C/C–ZrC (0.002 mm/s [20]), C/SiC–$ZrB_2$ (0.041 mm/s [10]), and C/SiC–TaC (0.038 mm/s [16]), the C/C–SiC–ZrC exhibits a good ablation resistance in high-temperature oxidant environments.

There are three typical ablation regions on the surface of C/C–SiC–ZrC composites: low temperature region, ablation center, and a region between them. Fig. 11a shows the morphology of the surface at low temperature region, in which the materials are slightly oxidized and no obvious mass loss. At the center of the ablated flame, the temperature can be 3000 °C [27], which results in the quick loss of silica. At such high temperatures, $ZrO_2$, the oxidation product of ZrC, will cover the fibers with the mixture of ZrC particles to prevent the fiber from being oxidized (Fig. 11c). Between the center and low-temperature zone, the temperature is in the range of 1700–2700 °C [20], and the mixture of Si–Zr–O amorphous glass can form dense layer for the protection of the composites (Fig. 11b). The good ablation resistance of the C/C–SiC–ZrC composites results from the protection of these oxides.

## 4. Conclusion

C/C–SiC–ZrC composites were fabricated by RMI process with molten $Si_{0.87}Zr_{0.13}$ alloy into the porous C/C preform. A unique structure of fiber tows covered by deposited carbon and SiC, followed by gradient ZrC–SiC was formed. C/C–SiC–ZrC composites showed a high bending strength due to the gradient matrix, which leads to the suppression of the cracks. The oxidation resistance of C/C–SiC–ZrC has been greatly enhanced compared to the C/C–ZrC composites because the

formed $SiO_2$ by oxidation of SiC can effectively prevent oxygen from attacking the carbon fiber inside. Due to the gradient SiC–ZrC matrix, the ablation properties of C/C–SiC–ZrC in oxyacetylene flame have no obvious reduction compared with C/C–ZrC composites.

## Acknowledgements

The authors would like to express their thanks to the reviewer for the explanation of the formation of SiC–ZrC gradient matrix.

This work is financially supported by the Chinese Natural Science Foundation (Grant # 51172181), the Research Fund of State Key Laboratory of Solidification Processing (NWPU) (Grant # 21-TP2007), and ''111'' project (B08040).

## References

[1] T.M. Besmann, B.W. Sheldon, R.A. Lowden, D.P. Stinton, Vapor phase fabrication and properties of continuous filament ceramic composites, Science 253 (1991) 1104–1109.
[2] S. Schmidt, S. Beyer, H. Knabe, H. Immich, R. Meistring, A. Gessler, Advanced ceramic matrix composite materials for current and future propulsion technology applications, Acta Astron. 55 (2004) 409–420.
[3] R. Naslain, A. Guette, F. Rebillat, R. Pailler, F. Langlais, X. Bourrat, Boron-bearing species in ceramic matrix composites for long-term aerospace applications, J. Solid State Chem. 177 (2004) 449–456.
[4] W. Krenkel, B. Heidenreich, R. Renz, C/C–SiC Composites for advanced friction systems, Adv. Eng. Mater. 4 (2002) 427–436.
[5] I. Toshihiro, K. Shinji, M. Kenji, H. Toshihiko, K. Yasuhiko, N. Toshio, A. Tough, Thermally conductive silicon carbide composite with high strength up to 1600 °C in air, Science 282 (1998) 1295–1297.
[6] F. Christin, Design, fabrication, and application of thermostructural composites (TSC) like C/C, C/SiC, and SiC/SiC composites, Adv. Eng. Mater. 4 (2002) 903–912.
[7] H. Li, L. Zhang, L. Cheng, Y. Wang, Fabrication of 2D C/ZrC–SiC composite and its structural evolution under high-temperature treatment up to 1800 °C, Ceram. Int. 35 (2009) 2831–2836.
[8] Y. Wang, Q. Liu, J. Liu, L. Zhang, L. Cheng, Deposition mechanism for chemical vapor deposition of zirconium carbide coatings, J. Am. Ceram. Soc. 91 (2008) 1249–1252.
[9] Q. Liu, L. Zhang, J. Liu, X. Luan, L. Cheng, Y. Wang, The oxidation behavior of SiC–ZrC–SiC-coated C/SiC minicomposites at ultrahigh temperatures, J. Am. Ceram. Soc. 93 (2010) 3990–3992.
[10] H. Li, L. Zhang, L. Cheng, Y. Wang, Ablation resistance of different coating structures for C/$ZrB_2$–SiC composites under oxyacetylene torch flame, Int. J. Appl. Ceram. Technol. 6 (2009) 145–150.
[11] Y. Wang, W. Liu, L. Cheng, L. Zhang, Preparation and properties of 2D C/$ZrB_2$–SiC ultra high temperature ceramic composites, Mater. Sci. Eng. A 524 (2009) 129–133.
[12] H. Hu, Q. Wang, Z. Chen, C. Zhang, Y. Zhang, J. Wang, Preparation and characterization of C/SiC–$ZrB_2$ composites by precursor infiltration and pyrolysis process, Ceram. Int. 36 (2010) 1011–1016.
[13] H. Li, L. Zhang, L. Cheng, Y. Wang, Oxidation analysis of 2D C/ZrC–SiC composites with different coating structures in $CH_4$ combustion gas environment, Ceram. Int. 35 (2009) 2277–2282.
[14] N. Padmavathi, S. Kumari, Prasad V.V. Bhanu, J. Ray, K.K. Subrahmanyam, Processing of carbon-fiber reinforced (SiC + ZrC) mini-composites by soft-solution approach and their characterization, Ceram. Int. 35 (2009) 3447–3454.
[15] Z. Wang, S.M. Dong, X.Y. Zhang, H.J. Zhou, D.X. Wu, Q. Zhou, D.L. Jiang, Fabrication and properties of $C_f$/SiC–ZrC composites, J. Am. Ceram. Soc. 91 (2008) 3434–3436.
[16] Y. Wang, Y. Xu, Y. Wang, L. Cheng, L. Zhang, Effects of TaC addition on the ablation resistance of C/SiC, Mater. Lett. 64 (2010) 2068–2071.
[17] Z. Chen, X. Xiong, G. Li, Y. Wang, Ablation behaviors of carbon/carbon composites with C–SiC–TaC multi-interlayers, Appl. Surf. Sci. 255 (2009) 9217–9223.
[18] L. Li, Y. Wang, L. Cheng, L. Zhang, Preparation and properties of 2D C/SiC–$ZrB_2$–TaC composites, Ceram. Int. 37 (2011) 891–896.
[19] L. Zou, N. Wali, J. Yang, N. Bansal, Microstructural development of a $C_f$/ZrC composite manufactured by reactive melt infiltration, J. Eur. Ceram. Soc. 30 (2010) 1527–1535.
[20] Y. Wang, X. Zhu, L. Zhang, L. Cheng, Reaction kinetics and ablation properties of C/C–ZrC composites fabricated by reactive melt infiltration, Ceram. Int. 37 (2011) 1277–1283.
[21] L. Brewer, O. Krikorian, Reactions of refractory silicides with carbon and nitrogen, J. Electrochem. Soc. 103 (1956) 38–51.
[22] D.R. Lide, Handbook of Chemistry and Physics, 79th ed., CRC Press, Boca Raton, FL, 1998.
[23] Y. Wang, Processing and Ablation Performance of TaC ($ZrB_2$) Modified C/SiC Composites. Degree thesis of Northwest University, Xi'an, 2011.
[24] E.K. Stroms, The Refractory Carbides, Refractory Materials, vol. 2, Academic Press, London, 1997.
[25] L.E. Toth, Transition Metal Carbides and Nitrides, Academic Press, New York, 1971.
[26] J. Jitcharoen, N.P. Padture, E.A. Giannakopoulos, S. Suresh, Hertzian-crack suppression in ceramics with elastic-modulus-graded surfaces, J. Am. Ceram. Soc. 81 (1998) 2301–2308.
[27] H. Zhou, R. Singh, Kinetics model for the growth of silicon carbide by the reaction of liquid silicon with carbon, J. Am. Ceram. Soc. 78 (1995) 2456–2462.